Urban Climate 47 (2023) 101351

Contents lists available at ScienceDirect

Urban Climate

journal homepage: www.elsevier.com/locate/uclim

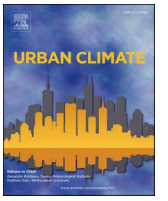

Observations of the urban boundary layer in a cold climate city

Mikhail Varentsov [a,b,c,*], Pavel Konstantinov [a], Irina Repina [a,b,c], Arseniy Artamonov [b], Alexander Pechkin [d], Andrei Soromotin [e], Igor Esau [f,h], Alexander Baklanov [g]

[a] Research Computing Center/Faculty of Geography, Lomonosov Moscow State University, Leninskiye Gory, 119991 Moscow, Russia
[b] A.M. Obukhov Institute of Atmospheric Physics, Pyzhevskiy Pereulok, 3, 119017 Moscow, Russia
[c] Moscow Center for Fundamental and Applied Mathematics, GSP-1, Leninskie Gory, 119991, Moscow, Russia
[d] Arctic Research Center of the Yamal-Nenets Autonomous District, Nadym, Russia
[e] Institute of Ecology and Natural Resources Management, Tyumen State University, 625000 Tyumen, Russia
[f] UiT – the Arctic University of Norway, 9037, Tromsø, Norway
[g] World Meteorological Organization (WMO), 7bis Avenue de la Paix, 1211, Genève, Switzerland
[h] Nansen Environmental and Remote Sensing Center, 5007, Bergen, Norway

ARTICLE INFO

Keywords:
Urban heat island
Urban boundary layer
Winter
Inversion
Cold spell
Drone
Quadcopter
ABL
UHI
UBL
UAV

ABSTRACT

Cold environment supports a large diversity of local climates. Among them, urban climates in northern cities stand out for their pronounced warm temperature anomaly known as the Urban Heat Island (UHI). UHI in northern cities has been already studies through satellite images and in-situ observations in the urban canopy layer (UCL). Yet, the vertical structure of the urban atmospheric boundary layer (UBL) has not been studied there. This work presents new observations of UBL in Nadym – a sub-Arctic Siberian city. During several intensive observing periods we run simultaneous registration of urban and rural meteorological parameters with unmanned drones, a microwave temperature profiler and a dense network of ground-based sensors. The data analysis reveals details of UHI development in the UCL and UBL, and links together horizontal urban-rural canopy-layer temperature differences, boundary layer stability, and UHI vertical extent. We show that during strong temperature inversions, UBL is less stratified than its rural counterpart, but it still remains very thin and limited in height by a few tens of meters. The observations disclose that the ground-based (50 m – 100 m above ground) temperature inversion is one of the strongest control factors for UHI in cold climate conditions in winter.

1. Introduction

Cities transform their environment and local climates. Urban surfaces are modified, aerodynamically rough, often physically impervious, and spatially heterogeneous. Those factors along with intense anthropogenic heat release create significant local climate anomalies at the surface and in the lower atmosphere (Oke et al., 2017). An urban heat island (UHI) – a climate effect of persistent urban temperature anomalies – is well known. But cities exhibit not only UHI near the surface. They also modify humidity, cloudiness and precipitation (Han et al., 2014; Varentsov et al., 2018b; Liu and Niyogi, 2019), wind regime (Droste et al., 2018), and other meteorological, hydrological and chemical parameters. Warm temperature anomalies could be found below cities in the active soil

* Corresponding author at: Research Computing Center, Lomonosov Moscow State University, Leninskiye Gory 1/4, 119234 Moscow, Russia.
E-mail address: mikhail.varentsov@srcc.msu.ru (M. Varentsov).

https://doi.org/10.1016/j.uclim.2022.101351
Received 21 March 2022; Received in revised form 3 September 2022; Accepted 15 November 2022
Available online 30 November 2022

layer (Lokoshchenko and Korneva, 2015) and in ground waters (Benz et al., 2016). Those climate factors directly or indirectly impact human wellbeing and economy.

Both warmer air and higher urban canopy roughness support generation of turbulent eddies and enhance turbulent mixing in the atmospheric boundary layer (ABL) over cities. Here, large urban-induced meteorological disturbances cannot be blended easily at some height within ABL. They are responsible for a distinct urban boundary layer (UBL). A typical UBL is commonly depicted as a relatively warm and polluted turbulent dome over a city (Oke et al., 2017; Fan et al., 2018). It maintains breeze-like mesoscale circulations induced by the city as whole (Lemonsu and Masson, 2002; Varentsov et al., 2018b). Urban heating increases the UBL height in comparison to the rural ABL (Pal et al., 2012), and delays decay of atmospheric convection over cities (Barlow et al., 2015).

Urban climate is still largely studied through its footprints on the surface or at best on an urban canopy layer (UCL). The surface UHI (frequently referred to as SUHI) is convenient for satellite monitoring (Voogt and Oke, 2003; Zhou et al., 2018), whereas UCL UHI is observed with in situ instruments. UBL UHI is expected to be observed within the whole UBL, e.g. Oke et al., (2017) defines it as a difference of the average temperature in the layer between the top of the UCL and the top of the UBL, and that at similar elevations in the rural ABL. Only a very few studies attempt to combine observations of SUHI, UCL, and UBL (e.g., Hu and Brunsell, 2015). This situation is perhaps unsurprising. Indeed, upper UBL could be inaccessible for direct observations. Low aircraft flights and meteorological balloons are usually not allowed in the urban areas. Meteorological masts and ground-based remote sensing instruments such as sodars and microwave radiometers may not reach upper UBL. Existing concepts of the UBL structure and variably is supported by only few fragmented observational studies (e.g. Bornstein, 1968; Oke and East, 1971; Oke, 1995; Lokoshchenko et al., 2016), and by several studies based on numerical modelling (Wouters et al., 2013; Varentsov et al., 2018a) or coarse-resolution remote-sensing data (Gorlach et al., 2018). A number of idealized theoretical and modelling studies of the urban heat dome have been published in the recent years that however do not address any realistic atmospheric stability and urban-rural temperature contrasts (Fan et al., 2017, 2020).

Looking for accessible UBL for observations, we turned our attention to cold (boreal) climate cities. The cold climate cities are found in boreal climate zones with temperatures below freezing and persistent snow cover over a significant part of the year as defined by Järvi et al. (2017) and Qian et al. (2022). Here, persistent surface energy deficit in wintertime creates stronger surface layer stability; it suppresses the turbulent mixing making UBL rather shallow, and therefore, more accessible for available instruments. Frequent anticyclonic weather conditions maintain calm wind, pronounced temperature inversions in the lower atmosphere (Wetzel and Brümmer, 2011), and a thin stable ABL (Davy, 2018). Thus, the UBL features are expected to become more contrast; UHI magnitudes to increase, and capping temperature inversion at the UBL top to sharpen.

Urban meteorology of cold climate cities is still poorly studied. Research publications are scarce (Brozovsky et al., 2020; Qian et al., 2022) and the cities are underrepresented in open access data sets (Chakraborty and Lee, 2019). Increasing interest to the Arctic region prompted new studies of the cold cities. These new studies were mainly based on analysis of land surface temperature (LST) from satellite data products, notably from the MODIS LST products (Esau et al., 2016, 2021; Miles and Esau, 2017). In situ data were collected through the UHIARC network in several Russian Arctic cities (Konstantinov et al., 2018; Varentsov et al., 2018a), and through observational networks in Barrow, Alaska (Hinkel and Nelson, 2007; Klene et al., 2013). Listed studies reveal significant SUHI and UCL UHI even in small and medium-sized cold climate cities. Here, SUHI and UCL UHI are typically amplified during winter cold spells, see, e.g., a comprehensive review of the Arctic urban climate studies in (Esau et al., 2021). Yet, the UBL in cold climate cities has been never investigated, except studies for Helsinki (Wood et al., 2013) with its relatively mild climate.

The present study makes the next step and extends urban climate research in high-latitude cities towards the UBL. We report a new data collection that discloses horizontal urban-rural meteorological differences, UHI vertical extent, and UHI dependence on atmospheric stability. Those factors allow characterization of the entire UBL. This study is done in a high-latitude city of Nadym in Russia under very cold winter conditions. To collect the data, we used several traditional (meteorological stations and sensors) and new instruments, namely, unmanned aerial vehicles (UAVs or just drones) and meteorological temperature profilers (MTP). Measurements were performed over several winters during shorter intensive observational periods (IOPs). The presentation has the following structure. The next Section 2 describes the study area, data collection and processing methodology and routines. Section 3 presents results including the vertical profiles of the UBL obtained by different instruments. Section 4 opens for discussion of the results and methodology. The last Section 5 highlights our conclusions.

2. Data and method

2.1. Study area

Nadym (about 45.000 inh.) is a typical example of Arctic urbanization in Russia. The city is located at 65.53° N, 72.52° E in Western Siberia just about 100 km to the south of the Arctic Circle. It is situated on a flat plain of the Nadym river alluvial terrasse. The elevation differences at and around the city do not exceed a few meters. The urban area is mainly built up with apartment buildings of 5 to 9 floors. Urban layout is compact with well-defined urban boundaries, which make the city well-suited for urban climate studies.

Over the last decade, Nadym has emerged as a research base for urban and peri-urban field studies in multiple scientific disciplines. One can mention permafrost studies related to CALM programme (Obu et al., 2019; Vasiliev et al., 2020), ecosystem studies on sandy outcrops (Sizov and Lobotrosova, 2016) and former wildfire sites (Sizov et al., 2021), micro-meteorological (Soromotin et al., 2021) and urban climate studies (Miles and Esau, 2017), as well as a row of holistic socio-environmental studies (Kumpula et al., 2011; Stammler and Sidorova, 2015; Yu et al., 2015; Fedorov et al., 2021).

Nadym is one of a few polar Eurasian cities covered by urban meteorological observations within the UHIARC field campaign

running since 2016 (Konstantinov et al., 2018). It justifies our selection of this city for more comprehensive UBL observations. Previous urban climate studies in Nadym (Miles and Esau, 2017; Konstantinov et al., 2018; Esau et al., 2021) reveal significant SUHI and UCL UHI in this small-size compact city. The published works have addressed UHI intensity, its spatial footprint, and relationships with specific weather conditions. Besides, Konstantinov et al. (2018) described in situ UHIARC observations and spatiotemporal variability of UCL UHI. Esau and Miles (2018) described the routines for MODIS LST processing, which differ from those adopted in (Chakraborty and Lee, 2019) global SUHI dataset where Nadym is not present.

In order to investigate the linkages between UCL, UBL and UHI, we organized five intensive observational periods (IOPs). Long-term UHIARC observations in Nadym were supplemented by extended ground-based observations and boundary layer profiling with drones and microwave temperature profiler (MTP). We describe our instruments and observational methodology below.

2.2. Ground-based measurements

Background meteorology of the Nadym area is observed at the only regular weather station of the World Meteorological Organization (WMO) with the station identification number 23445. The station is located near a landing strip of the Nadym airport at about 10 km from the city (WMO site at Fig. 1) and represents the background (non-urban) climatic conditions. The WMO station data are freely available at 3-hourly frequency; data with 1-min frequency during the selected IOPs was additionally requested for this study.

Urban meteorological parameters are also registered by a Davis Vantage Pro 2 automatic weather station (AWS), which is installed in a central city park (AWS1 site in Fig. 1). The park is rather small and has a rarified tree stand (Fedorov et al., 2021), so it would likely have only a limited effect on local climate (Xiao et al., 2018). The station is in operation since 2016 as a part of the UHIARC network (Konstantinov et al., 2018). Since 2020, the urban network in Nadym was expanded with new AWS2 and AWS3 of the same type as AWS1. AWS2 was installed in a courtyard surrounded by densely built 9-storey blocks. AWS3 was installed within a low-rise industrial part of the city. Observational frequency for AWSs is 5 min. All AWSs are supplemented by Onset Hobo MX2300 gradient temperature loggers (Hobo TLs) with sensors at 1.5 and 3 m. Data from these TLs was used to fill temperature gaps in AWS data, including the cases when temperate drops below -40 °C, which is the lowest limit of the AWS measurement range.

During most of IOPs, the ground-based network was enhanced by compact iButton temperature loggers (iButton TLs) deployed within and outside the city (Fig. 1). iButton TLs were installed on low bush branches at about 2 m above the surface. Our previous UHIARC studies proved that TLs even without radiation shields can provide reliable temperature observations when the sun is low or absent (Konstantinov et al., 2018; Varentsov et al., 2018a). Since such conditions are found during the major part of the reported observational periods (the polar winter), the use of TLs without shielding is justified. Observational frequency for TLs varied from 5 to 30 min in different years.

The temperature differences at AWSs or TLs and WMO sites, $\Delta T_i = T_i - T_{WMO}$, quantify the UCL UHI intensity.

2.3. ABL profiling

The novelty of our study lies in using unmanned drones for nearly simultaneous observations of the ABL structure within and outside a city. The first attempts of using UAVs for atmospheric research go back to 1970s (Konrad et al., 1970), and nowadays both fix-wing and rotary-wing drones are widely used for ABL research (Bell et al., 2019; Chilson et al., 2019; Kral et al., 2021). Rotary-wing

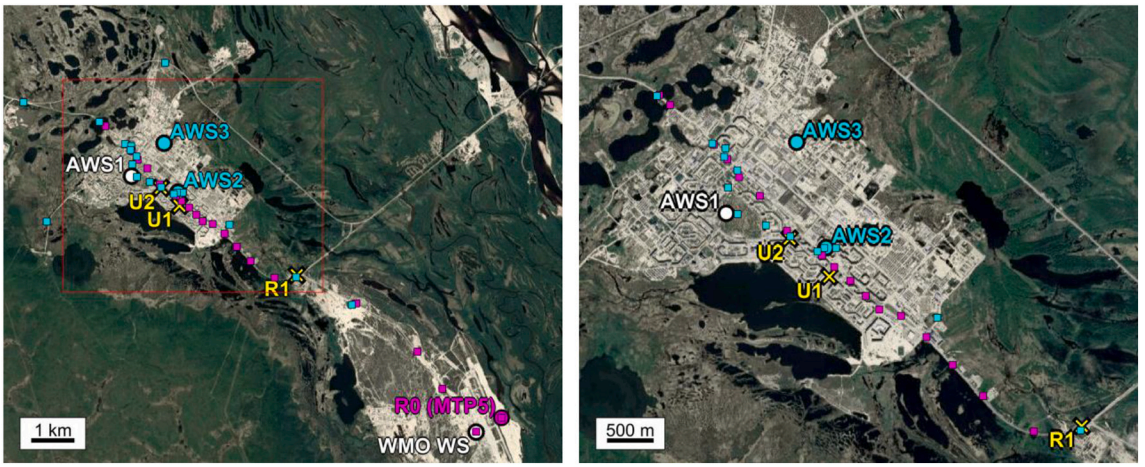

Fig. 1. The deployed observational network in Nadym. White color indicates sites with long-term ground-based observations. These observations are available for the whole considered period. Magenta color indicates sites where extended observations were performed during IOP-1 in December 2018. Cyan color indicates extended sites operated during IOPs 3, 4 and 5 in 2021. Yellow color indicates sites where drones were used for atmospheric profiling. The left panel shows the Nadym and airport areas; the right panel zooms into the Nadym urban area. (For interpretation of the references to color in this figure legend, the reader is referred to the web version of this article.)

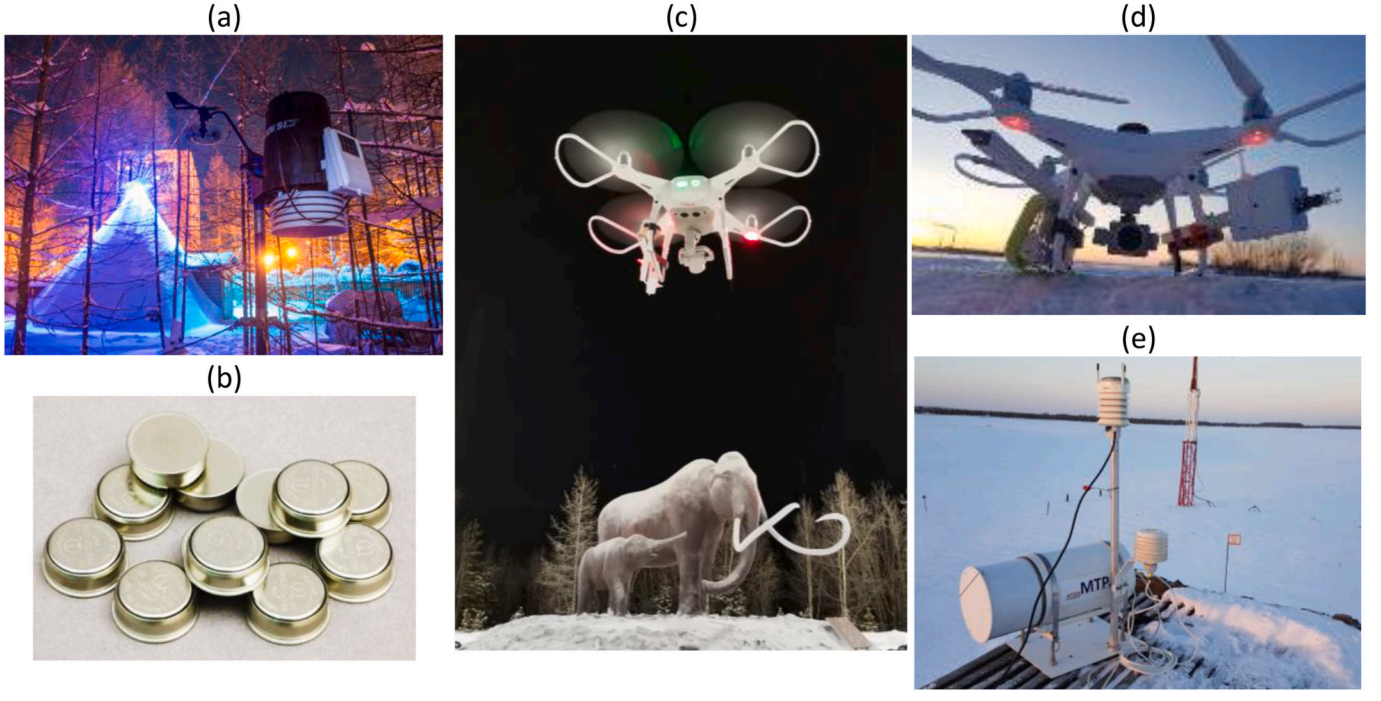

Fig. 2. The equipment used for the experimental atmospheric observations in Nadym: automatic weather station Davis Vantage Pro 2 at AWS1 site (a), iButton TLs (b), DJI Phantom 4 Pro drone at R2 site (c), more detailed photo of the drone and sensors (d), MTP-5 at R0 site (e).

drones, with their ability to hover and to slowly ascend and descend vertically, have clear advantages for accurate measurements in stable-stratified ABL (Kral et al., 2021; Tikhomirov et al., 2021). Another key advantage of the multi-rotor UAVs is an opportunity to estimate the wind speed and direction without any additional sensors using only altitude data (pitch and roll angles) from their internal measurement unit (Neumann and Bartholmai, 2015; Palomaki et al., 2017). High-end multirotor drones are already developed for the ABL research (Segales et al., 2020) and for the needs of automated atmospheric profiling (Leuenberger et al., 2020). At the same time, even the mass-market drones with attached meteorological sensors can provide high-resolution and accurate enough measurements of key meteorological parameters inside the ABL (Varentsov et al., 2019, 2021a; Kimball et al., 2020). Nevertheless, UAV applications in the UBL research remain rather new and limited to a few studies (Adkins et al., 2020; Sekula et al., 2021), with none considering cold winter conditions.

We use DJI Phantom 4 Pro quadcopters. These drones are equipped by meteorological sensor packages iMet-XQ2 and iMet-XF from Intermetsystems company (Fig. 2). iMet- XQ2 is a compact ready-to-use system that includes internal memory, GPS as well as a set of temperature, humidity and pressure sensors. iMet-XF sensor package is part of the customized system (Varentsov et al., 2019) that also includes a data logger and a power supply block (packed in a plastic box), and a NTC temperature sensor. Observation frequency for both sensor packages is 1 s. Declared accuracy of all listed temperature sensors is ±0.3 °C. Both sensor packages are mounted at chassis under the drones; the sensors are placed under the front rotors for better aspiration (Fig. 2). A dataset for each vertical profile consists of sequential ascent and descent with vertical speed of about 0.5 m/s in the lowest 50 m and 1–1.5 m/s above. The measurements were collected between 120 m and 250 m (depending on weather conditions and radio interference). Each individual sounding typically takes about 10 min.

Processing of the drone-based measurements involves sensors' readings and drone's flight logs. The workflow includes synchronizing data from the sensors and the flight logs, identifying take off/landing time and ascending/descending flight segments, and determination the height over the ground based on pressure and temperature readings. Data processing includes correction for inertia of the sensors and resulted hysteresis pattern in the vertical profiles measured on ascend and descend (Varentsov et al., 2019; Tikhomirov et al., 2021). We correct such effect by shifting the observed time series by a lag Δt, which is determined for each separate sounding by minimizing the root-square difference between profiles observed on ascend and descend. For iMet-XQ2 and NTC temperature sensors, Δt varied from 0 to 8 s with mean value of 3.5 s. EE03 sensor has larger inertia with typical Δt about 6–9 s. Data processing also includes estimation of wind speed and direction from the drone's flight logs as described in (Varentsov et al., 2021b). Finally, data processing routines provides vertical profiles of the temperature, humidity, pressure, wind speed and direction, averaged over ascending and descending segments. The obtained temperature and pressure readings are further converted to potential temperature (θ) profiles which are more useful for stratification analysis.

We also use a microwave temperature profiler MTP-5 from the ATTEX company (http://mtp5.ru/). MTP-5 is a passive scanning radiometer retrieving the air temperature in the elevation range from 0 m to 1000 m above the ground (Kadygrov and Pick, 1998). It retrieves temperature profile from microwave brightness temperature measured at difference angles solving inverse problem. The lower point temperature in MTP-5 is measured by independent temperature sensor (shielded from radiation) outside the instrument. It is used then as a reference temperature for retrieval algorithms that convert the registered brightness temperature to the meteorological absolute temperature. Declared accuracy of MTP-5 temperature measurements (root-mean square error) is 0.2–1.2 K. Vertical resolution of the MTP-5 data is 25 m in the lowest 100 m layer and 50 m above it. The measurement frequency is 5 min. Observations with MTP-5 as well as drones quantify atmospheric stability conditions and allows estimating vertical extent of the UBL UHI.

Table 1
Summary of intensive observational periods in Nadym.

IOP №	Period	Ground-based measurements*	ABL measurements
1	19–27 December 2018	• Urban AWS (AWS1 site) • Hobo gradient TLs at the urban (AWS1) and rural (WMO) sites • 22 iButton TLs • Radiation measurements with Kipp&Zonen instruments at the WMO site (CMP21 pyranometer, CGR4 pyrgeometers)	• Continuous observations of temperature profile by the MTP-5 profiler at the rural site R0 • 3 profile soundings over the city at the U1 site done with one drone equipped with iMet-XF & iMet-XQ2 sensors (P1.1-P1.3)
2	20–21 December 2019	• Urban AWS (AWS1 site) • Hobo gradient TLs at the urban (AWS1) and rural (WMO) sites	16 alternate profile soundings over the rural (R1) and urban (U2) sites done with one drone equipped by iMet-XQ2 sensor (P2.1 – P2.16)
3	9–11 January 2021	• 3 urban AWSs (AWS1–3) • Hobo gradient TLs at the urban (AWS1–3) and rural (WMO) sites • 18 iButton TLs	15 paired synchronous profile soundings over the rural (R1) and urban (U1/U2) sites done with two drones equipped by iMet-XQ2 sensors (P3.1–3.15)
4	5 February 2021		6 alternate profile soundings over the rural (R1) and urban (U2) sites done with one drone equipped by iMet-XQ2 sensor (P4.1–4.6, P5.1-P5.6)
5	13 February 2021		

* in addition to regular observations at the WMO site.

2.4. Intensive observational periods (IOPs)

Performing continuous observations in a remote city is an extremely resource-intensive task. Instead, we collected data during several IOPs. Table 1 presents basic information about these IOPs, including their duration and instrumentation, and Fig. 1 shows location of observational sites. Each IOP included at least a few drone-based profile measurements, further referred as Pi.j, where *i* is an IOP number, and *j* is a profile number during this IOP (e.g. P1.1 is the 1st profile measured during 1st IOP).

IOP-1 in December 2018 was the longest and included most detailed ground-based observations. In addition to AWS and 22 TLs, components of the surface radiation balance were monitored by Kipp & Zonen instruments (CMP21 pyranometer for downwelling shortwave flux, CGR4 pyrgeometers downwelling and upwelling longwave fluxes) at WMO site, and the temperature profile was continuously scanned by MTP-5 at the rural site R0 near the airport landing strip, at a distance of about 600 m from WMO site (Fig. 2). R0 site was located within a flat and open snow-covered area between the landing strip and forest, far away from buildings and other sources of anthropogenic heat. The MTP-5 instrument was placed at the roof of a metal container at approximately 3 m height above the surface (Fig. 2). The R0 observations were also supplemented by Vaisala WXT520 AWS. However, during IOP-1 the drones were operated only within the city at the U1 site found at a wide boulevard between 9-storey blocks (Fig. 2). We managed to complete only 3 successful profiles.

The following IOPs were aimed to extend data sampling and to perform fully comparable profile measurements with drones at both urban and rural sites. During IOP-2 (December 2019), we performed measurements using one drone with the iMet-XQ2 sensor. The drone was launched alternately at two points, the rural site R1 in 4 km from the city, and the urban site U2 located at an open area with a roundabout (Fig. 1). We managed to obtain 16 soundings, with time difference between urban/rural soundings about 30 min. IOP-2 data collection did not include any ground-based observations additional to long-term network, but next IOPs were supported by extended network consisting of two new AWSs and 18 iButton TLs. During IOP-3 (9–10 January 2021) we performed 15 paired synchronous soundings at the urban and rural sites using two drones equipped with the iMet-XQ2 sensors. The R1 site was again used as a rural site, and the U1 and U2 sites were alternately used for profiling over the city to cover different types of the urban environment. Very short IOP-4 and IOP-5 were organized in February 2021 to extend the data sampling adding more cases with strong intensive cold spells and strong UHI. IOP-4 and IOP-5 consisted of 6 alternate soundings each over the rural (R1) and urban (U2) sites. These soundings were performed with a 30-min interval.

2.5. Larger-scale weather conditions

To illustrate the large-scale weather conditions, we use the state-of-the-art ERA5 reanalysis data from ECMWF (Hersbach et al., 2020). Its spatial resolution is 0.25° (approx. 30 km), temporal resolution is 1 h. Since our IOPs provide relatively short samplings of wintertime weather conditions, ERA5 reanalysis was used to investigate relationships between observed UBL UHI and a set of large-scale control parameters. We consider the following parameters derived from ERA5: wind speed at 10-m height, V_{10m}; the mean wind speed in the layer, $\overline{V_z}$;the ABL height, H_{ABL}, (blh ERA5 variable), defined as the minimum height for the bulk Richardson number reaching the value of 0.25 according to (Vogelezang and Holtslag, 1996); net thermal radiation, Q_L, (str ERA5 variable); and strength of the ground-based temperature inversion, ΔT_z, in the lowermost layer with the thickness z ($z = 50$, 100, 200 and 300 m), i.e.,

$$\Delta T_z = \begin{cases} T_z - T_{2m}, T_z - T_{2m} > 0 \\ 0, T_z - T_{2m} \le 0 \end{cases}$$

We also use two parameters derived from observations at the WMO site, namely, 10-m wind speed, V_{10m}^{obs}, and a weather factor, F_W^{obs}, which is an empirical function from wind speed and cloud fraction suggested in (Oke, 1998). The weather factor was found to closely correlate with the UHI intensity in the Arctic cities (Konstantinov et al., 2018; Varentsov et al., 2018a). Here we use the same definition as in previous UHIARC studies:

$$F_W^{obs} = \left(1 - 0.8n_t^2 - 0.4(n_t - n_l)^2\right) \bullet min\left(V_{10m}^{obs\ -\frac{1}{2}}; 1\right),$$

where n_t and n_l are observed total and low cloud fraction respectively.

We further analyzed the correlation between UCL UHI intensity according to long-term observations (ΔT_{AWS1}, ΔT_{AWS2}) and the listed variables. To deal with ambiguity associated with time difference between observations and reanalysis data, we consider time series smoothed with a 6-h running window. The correlations are obtained for the December–February months of 2018/19, 2019/20 and 2020/21 winter seasons (hereafter referred as P1 period) for ΔT_{AWS1}, and of 2020/21 season (hereafter referred as P2 period) for both ΔT_{AWS1} and ΔT_{AWS2}.

3. Results

We observed significant UHI during most of IOPs, yet its intensity and persistence varied strongly. Weather conditions and physical factors, such as ABL stratification, had a marked impact on the UHI and UBL characteristics. We consider those factors below.

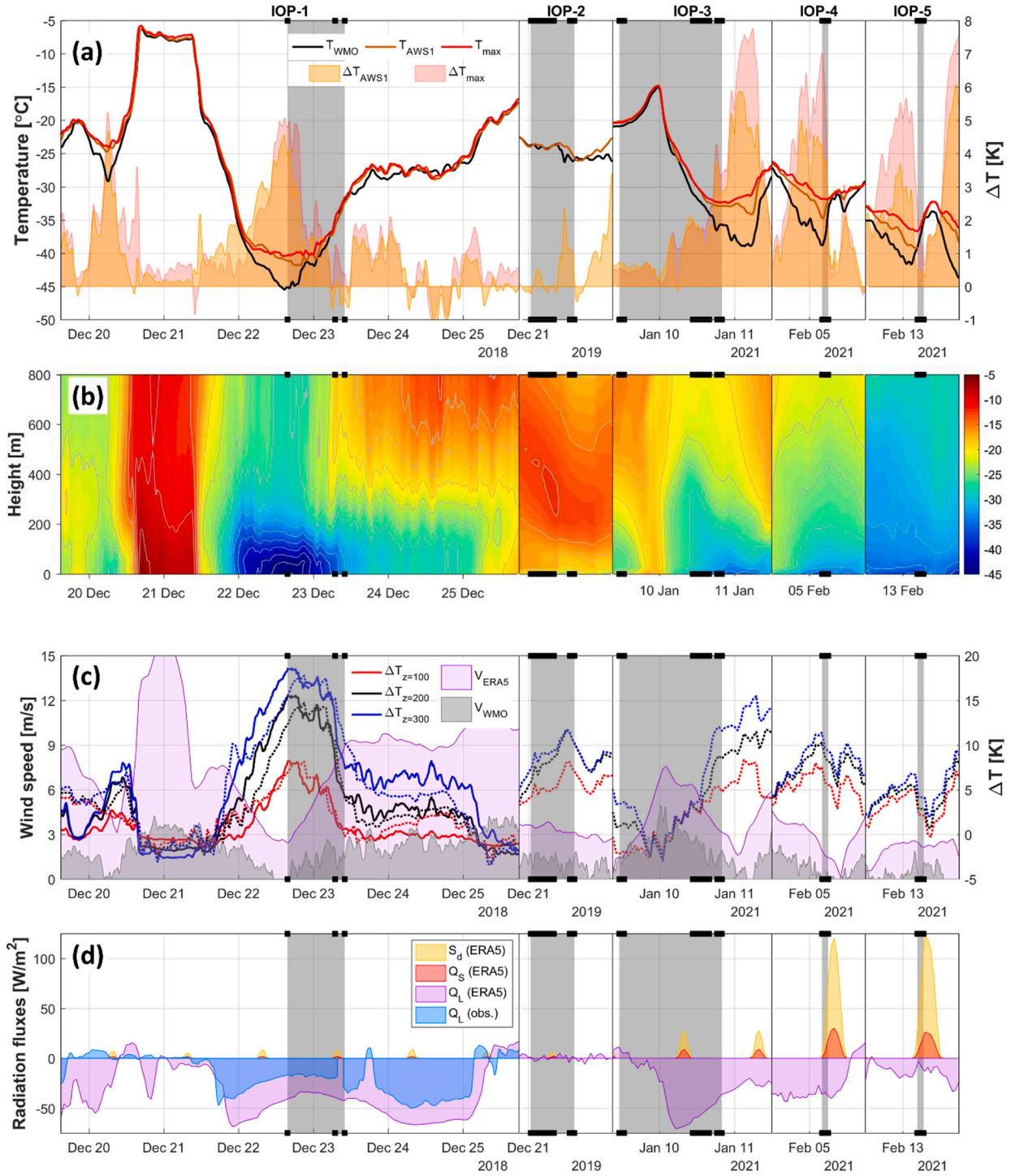

Fig. 3. Weather conditions during the intensive observational periods (IOPs): urban and rural air temperature and UCL UHI intensity for AWS1 site and for warmest urban site (T_{max} and ΔT_{max}, which correspond to TL near U1 site for IOP-1, to AWS2 for IOPs 3, 4 and 5) (a); temperature stratification according to MTP-5 observations for IOP-1 and ERA5 reanalysis for other IOPS (b); wind speed according to observations at WMO site and ERA5, vertical temperature differences ΔT_z for z = 100, 200 and 300 m according to MTP-5 observations (solid lines) and ERA5 (dotted lines) (c); downward (S_d) and net (Q_S) shortwave radiation according to ERA5, net longwave radiation Q_L according to ERA5 and observations (d). Time series are averaged with a 1-h running window. Gray strips indicate periods of vertical profiling (soundings) with drones, black squares on X-axis indicate exact time of such soundings.

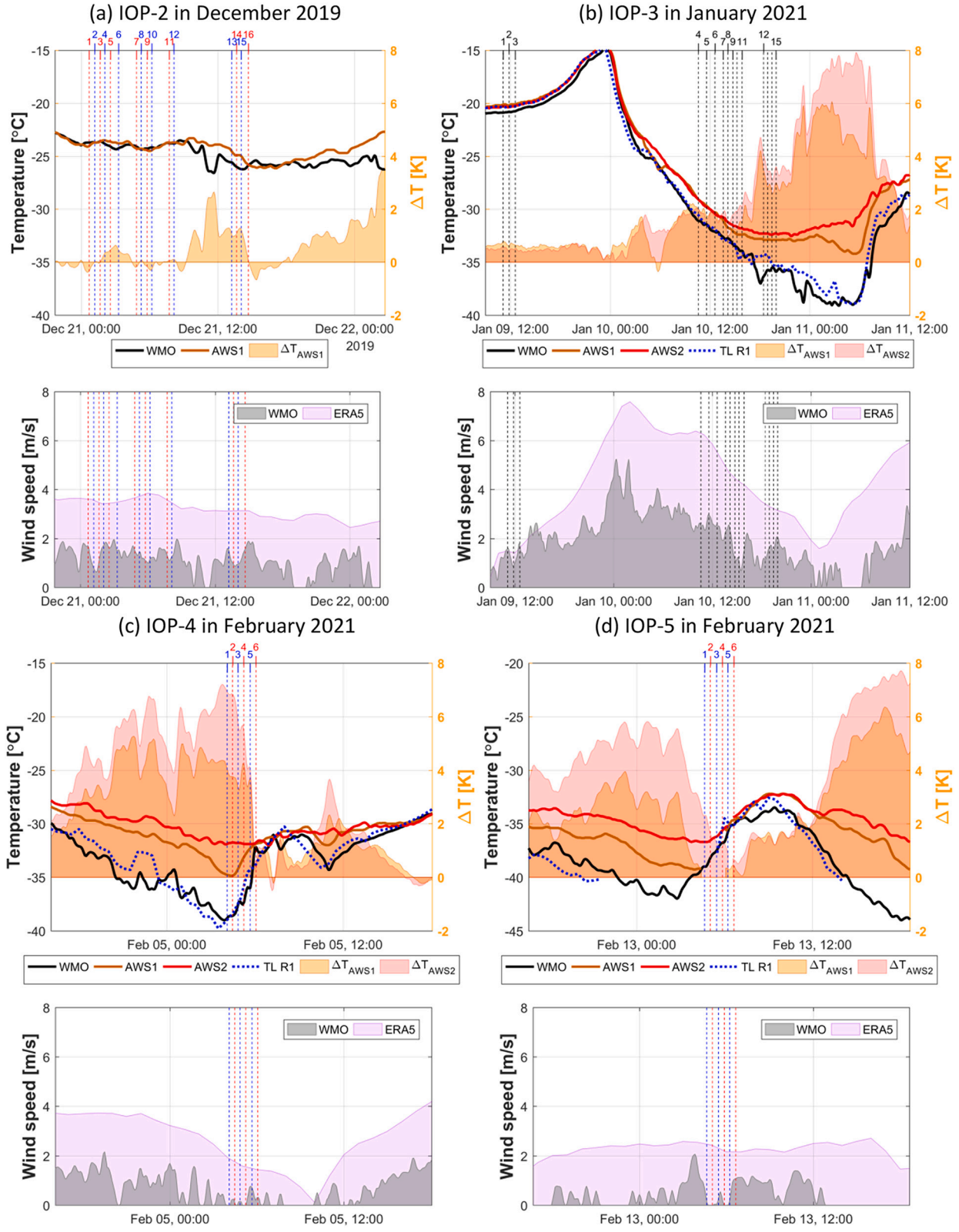

(caption on next page)

Fig. 4. Time series of air temperature, UCL UHI intensity and wind speed during IOP-2 in December 2019 (a), IOP-3 in January 2021 (b), IOP-4 and IOP-5 in February 2021 (c, d). Vertical dotted lines indicate the moments of the drone-based soundings in urban (red dotted lines) or rural (blue dotted lines) sites or paired simultaneous soundings in both sites (black dotted lines). (For interpretation of the references to color in this figure legend, the reader is referred to the web version of this article.)

3.1. Weather conditions and canopy-layer heat island during IOPs

Weather conditions observed during IOPs varied broadly. Several cold spells or periods with rapid cooling followed by frosty weather were observed (Fig. 3). The longest IOP-1 in December 2018 comprised two cold spells. The first, shorter cold spell on December 20, showed the rural temperature drop from −20 °C to −30 °C in 9 h. The second, longer cold spell (on December 22 to 25), showed the rapid temperature drop from −5 °C to −40 °C in 24 h, and then a slow colling to −46°C. During IOP-2, weather conditions were relatively stable with a slow cooling trend. By contrast, IOP-3 comprised rapid temperature changes, including warming on January 9, 2021, and a rapid temperature drop from −15 °C to −37 °C through the next day. Temperature dynamics observed in IOPs 4

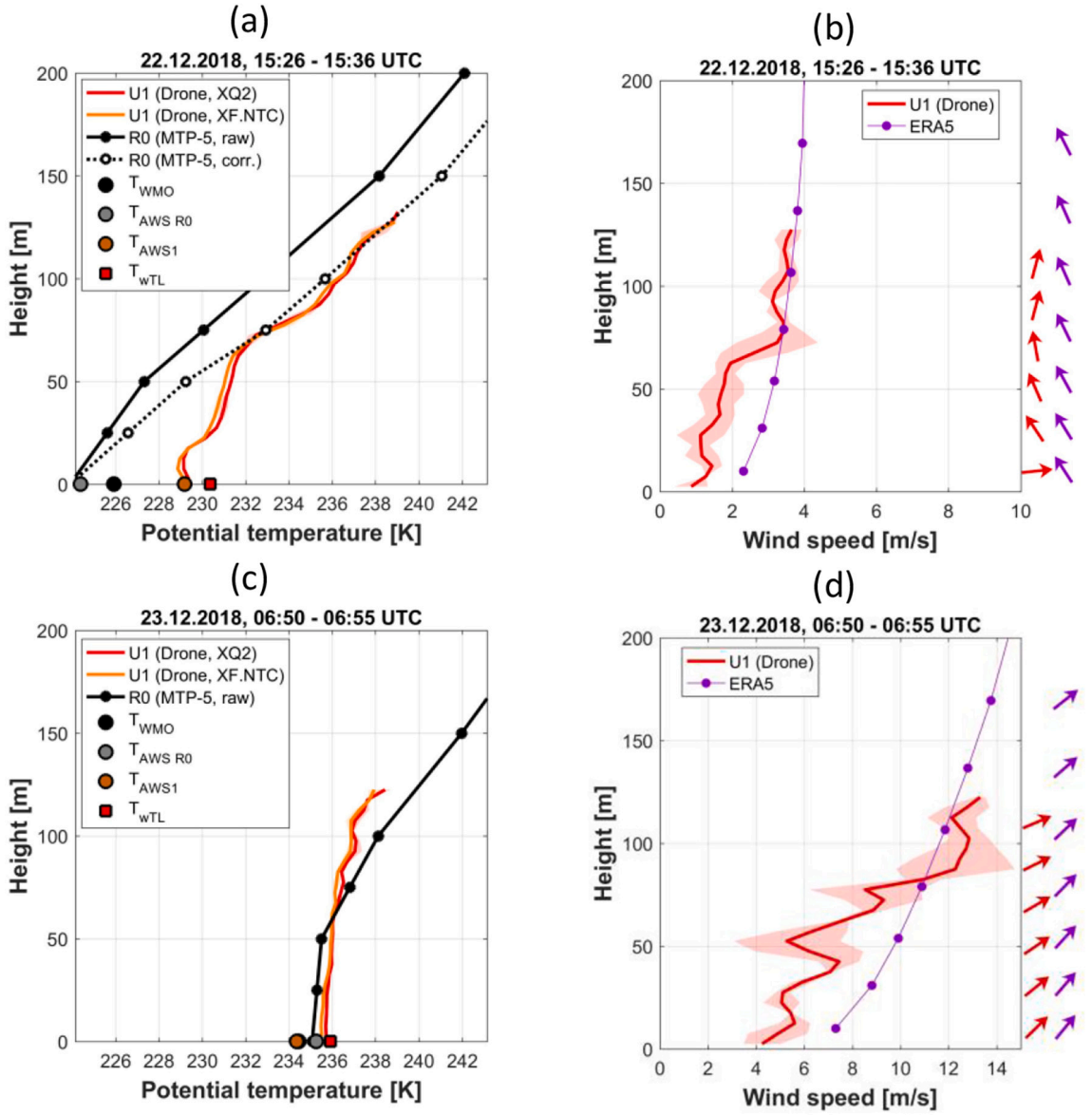

Fig. 5. The potential temperature (a, c) and wind speed (b, d) profiles obtained by drone sounding during the P1.1 (a, b) and P1.2 cases (c, d) in December 2018. Note the different scales for the wind speed axis for these two cases. Arrows to the left from wind speed plots indicate wind direction.

and 5 was close to IOP-3. A pronounced UCL UHI was recorded during all cold spells observed in IOPs 1, 3, 4 and 5, with its intensity reaching up to 7 K. UCL UHI intensity for the densely built areas (ΔT_{max} in Fig. 3, which corresponds for TL new U1 site for IOP1 and AWS2 for other IOPs) was typically by 0.5–2 K higher than for urban park (AWS1). Beyond the cold spells, UCL UHI intensity remained rather weak (typically lower than 2 K).

According to the MTP-5 observations available for IOP-1 and ERA5 reanalysis for other IOPs, the cold spells were accompanied by strong temperature inversions. The temperature increased in the lowest 300 m as much as 20 K for second cold spell in IOP-1, and by 8–15 K for other cold spells. Between the cold spells, periods with neutral or unstable stratification were also observed. It worth to note that IOP-1 data proved relatively good agreement between MTP-5 observations and reanalysis in terms of temperature stratification (correlation coefficient is 0.78, 0.9 and 0.92 for $\Delta T_{z=100}$, $\Delta T_{z=200}$ and $\Delta T_{z=300}$ respectively), justifying usage of the latter for other IOPs.

All observed cold spells were accompanied by the decrease in the wind speed, represented both by the local WMO observations and ERA5 reanalysis (Fig. 3). The observed wind speed was always lower than in reanalysis and dropped nearly to zero at the peaks of cooling. Downward (S_d) and net (Q_S) short-wave radiation was almost absent during IOPs 1, 2 and 3 as it was winter solstice time at a place near the Arctic circle (daylight duration during these IOPS did not exceed 3.5 h and solar elevation did not exceed 2.5°). Yet, these fluxes became significant during daytime hours in IOPs 4 and 5 in February (Fig. 3). The radiation balance was mostly controlled by net long-wave radiation (Q_L). Q_L was typically negative reaching -50 W m^{-2} at early time of the observed cold spells. Yet, it was close to zero between the cold-spells as well as during the whole IOP-2. IOP-1 data shows that observed Q_L dynamics is reasonably captured by the ERA5 data, with an overall negative bias and only significant discrepancies on December 20, just before the first cold spell.

We observe a good correspondence between the most intense UCL UHI periods and the periods of the strongest temperature inversions. Yet, the UCL UHI intensity is the best correlated with inversion strength in the lowest 100 m, while the presence of inversion in a thicker layer may not be accompanied by UHI. For example, after the peak of cooling on December 22, 2018, the $\Delta T_{z=300\,m}$ exceeds 5 K for two days, but the near-surface temperature gradient remained nearly zero and so UHI was rather weak. We also found good correspondence between wind speed, UHI intensity and the strength of near-surface inversions: both phenomena develop when the wind speed drops below 1 m/s in the WMO observations (below 4 m/s in the ERA5 data). All observed UHI cases were accompanied by radiative cooling and negative Q_L. Yet, despite faster radiative cooling of the rural surface is considered one of important factors for UHI (Oke, 1982), in our case there was no clear correlation between Q_L and UCL UHI intensity. For example, during the second cold spell in IOP-1, UCL UHI developed in 20 h after the minimum Q_L was observed.

We were able to cover a wide part of observed variety of weather conditions by drone-based soundings. In IOP-1, we obtained data at the peak of the cold period on December 22, 2018, when the strongest UCL UHI and the strongest inversion were observed. Then, we observed weaker temperature gradients at the next day. In IOP-2, we performed series of soundings against the weak UCL UHI with its intensity not exceeding 2 K (Fig. 4a). In IOP-3, we performed the first soundings (P3.1 - P3.3) before the cold spell when UCL UHI was absent, and next day we managed to cover by dense soundings (P3.4–3.15) the first part of cooling and UCL UHI development (Fig. 4b). The last two IOP-4 and IOP-5 (February 2021) were used to attempt for short measurements at the peak of the cold spell. These drone soundings were planned in accordance to weather forecast and real-time AWS observations. Yet, in both cases, we actually captured only the end of cold spells and the following transition periods with growing temperatures and decreasing UCL UHI (Fig. 4c, d).

3.2. Observed atmospheric boundary layer profiles

The first drone sounding for IOP-1 (P1.1) illustrates UBL for the case with lowest temperature and strongest inversion among all cases. It provided urban meteorological profiles up to 130 m at the U1 site (Fig. 5a,b). The urban temperature profile is compared with the rural profile from MTP-5 at the R0 site. The lower atmosphere at both sites is stable stratified. Yet, the lowest 50 m of air exhibit weaker stratification (the θ gradients are two times smaller) in the city than at the rural site (Fig. 5a), making possible to identify this

Fig. 6. The Aerial photo of Nadym city taken from the drone when performing vertical profiling for the P1.1 case on 22nd December 2018 (shown at Fig. 5a,b).

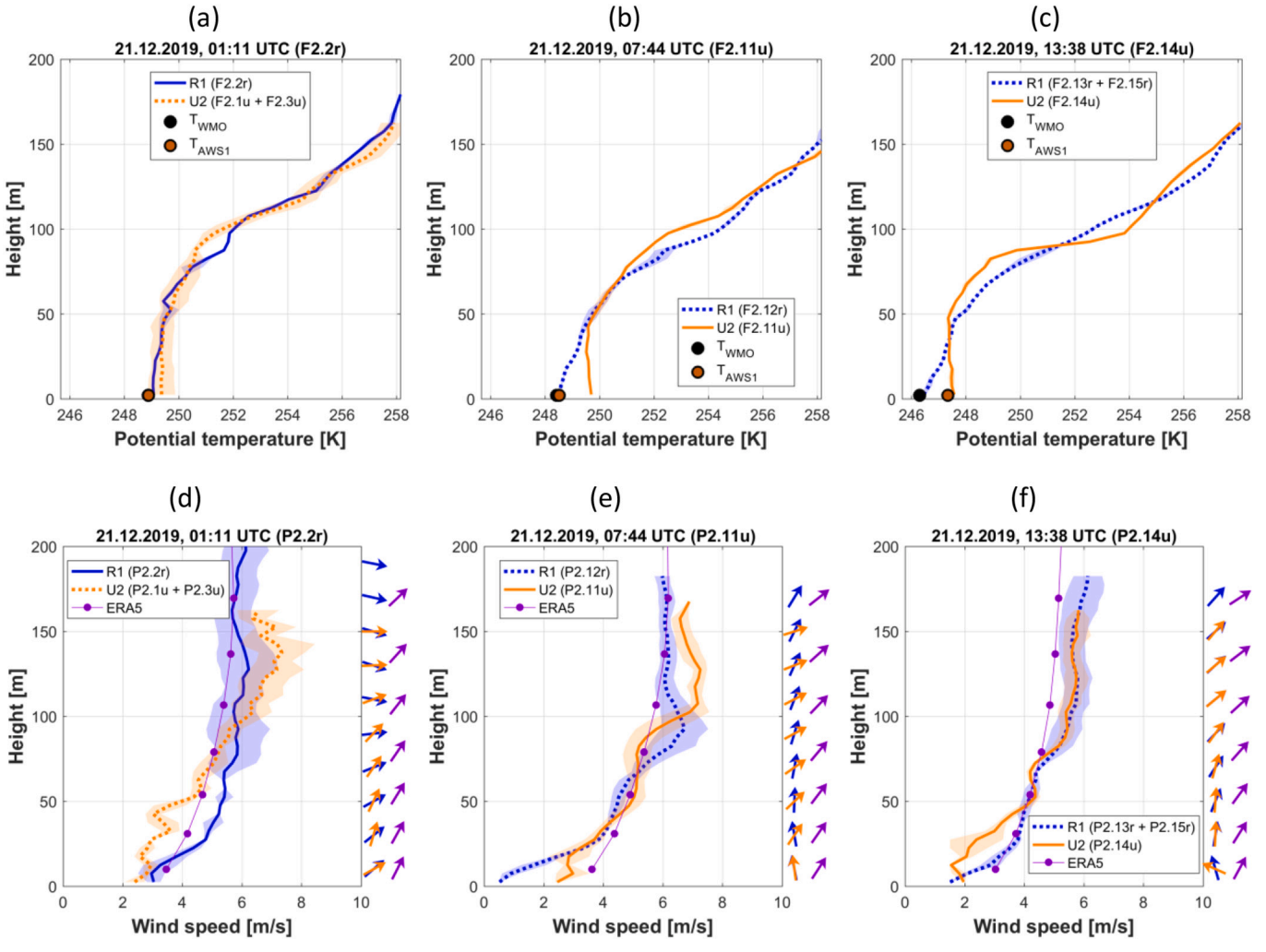

Fig. 7. Vertical profiles of potential temperature (a-c) and wind speed (d-e) obtained from drones at the R1 and U2 sites during IOP-2 in December 2019. The solid lines indicate the instant profiles; the dotted lines indicate the profiles averaged for two adjacent time moments. Arrows to the left from wind speed plots indicate wind direction.

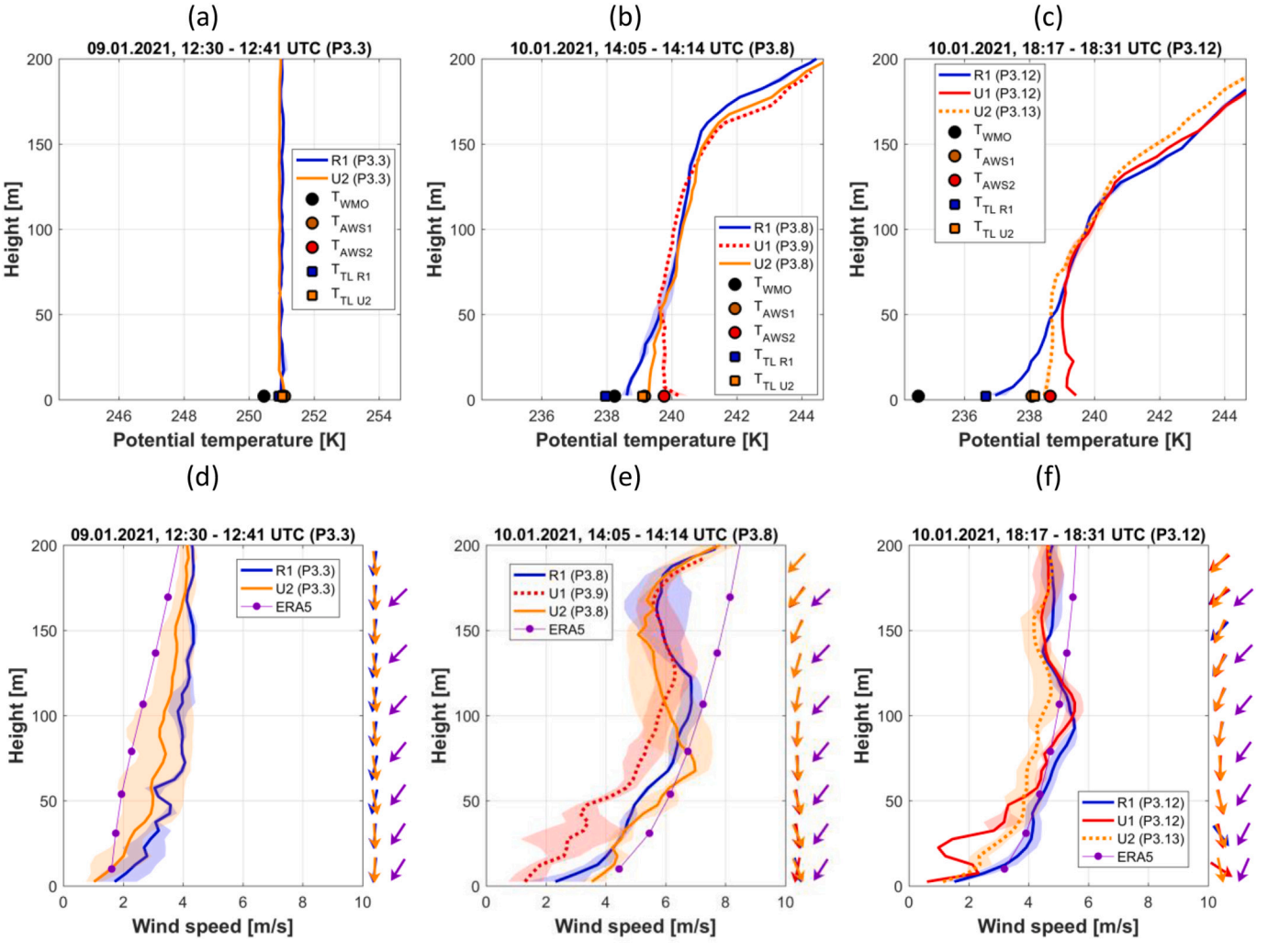

Fig. 8. The same as in Fig. 7 but for the IOP-3 in January 2021.

layer as UBL. Above the UBL (above 75 m) θ gradients were observed to be very similar. The fact that we used measurements from MTP-5 and drones explains differences in the temperature in whole air column up to 120 m. Drones measure the absolute temperature, and MTP-5 retrieves a relative changes of temperature profile. It is also known that MTP-5 tends to underestimate near-surface temperature gradients in stably-stratified conditions (Kadygrov et al., 2012; Ezau et al., 2013; Varentsov et al., 2019, 2021b). Considering this bias, the equality of gradients above the UBL and theoretical background (Claussen, 1991; Mahrt, 2000), we assume that both temperature profiles must coincide in the free atmosphere. Such assumption suggests a correction for MTP-5 bias, which is a constant above the 75 m and linearly decreases to zero at the surface. The corrected profile in Fig. 5a present the remaining temperature difference within UBL up to 50–75 m above ground, which we interpret as the UHI vertical extent. An additional indirect support of our UBL height identification is drown from analysis of a fog layer that was observed at that time over the city. Aerial image (Fig. 6) and video recorded from the drone during its ascent identify the depth of fog layer as about 50 m. Drone-estimated wind profile together with ERA5 data show that such a strong ground-based inversion and UHI develop against a background of low, but non-zero wind speed not exceeding 3 m/s in the lowest 50 m (Fig. 5b).

Two next soundings (P1.2, P1.3), were performed later on December 23. Their data shows the presence of mixed layer over the city as well as over rural area, without any significant differences between two sites, and much stronger wind that at previous case (Fig. 5c, d).

The next IOPs provided more consistent profiles obtained by drones launched at both urban and rural sites. The IOP-2 data illustrates the ABL evolution during a slow cooling event. At the beginning of IOP-2, there was a mixed layer in the lowest 75 m and a strong elevated inversion above (Fig. 7a). Further into the cooling event, the elevated inversion became stronger and lowered, and a

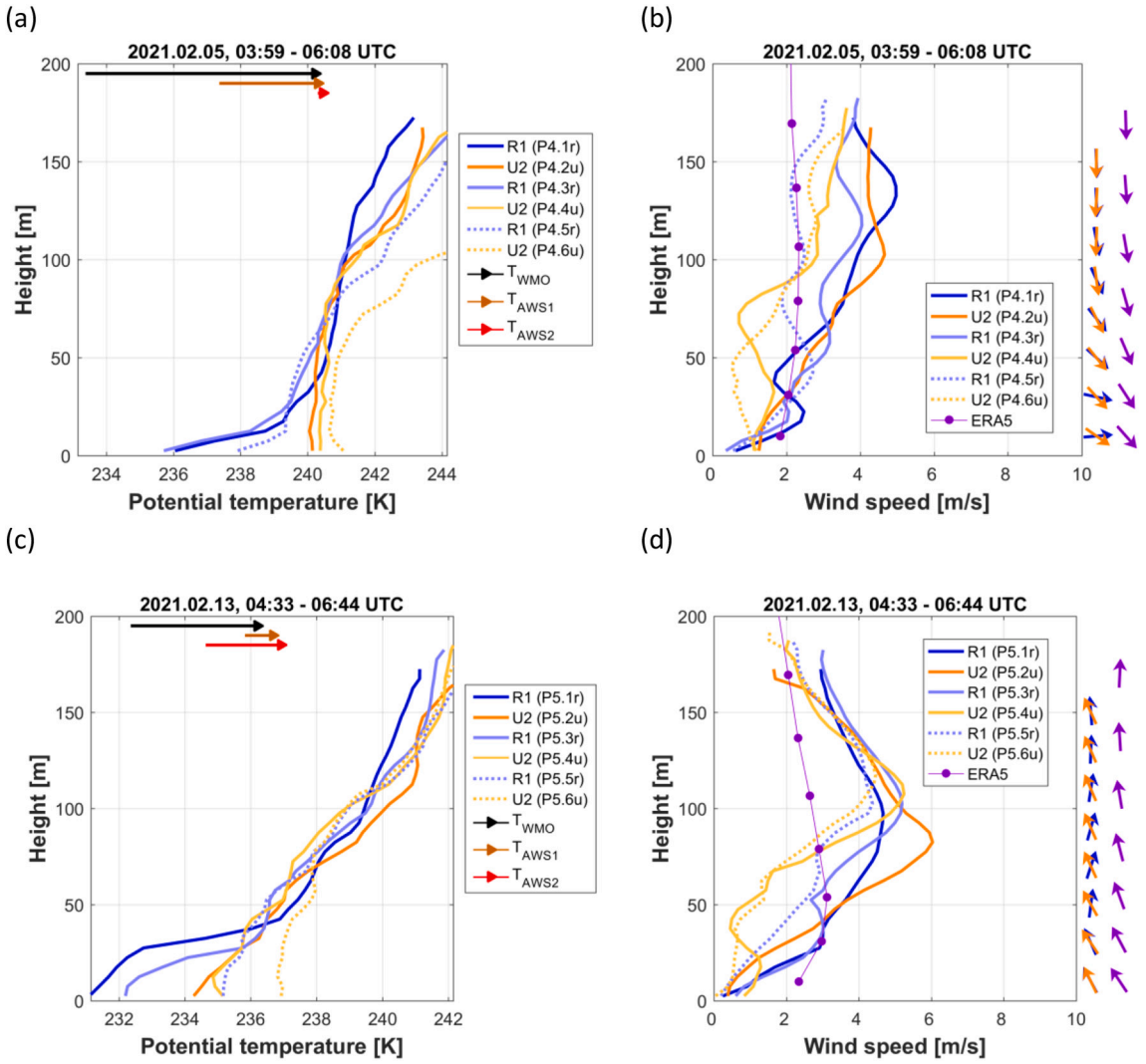

Fig. 9. Vertical profiles of potential temperature (a, c) and wind speed and direction (b, d) according to drone-based soundings in R1 and U2 sites during IOPs 4 and 5 in February 2021. Arrows at temperature plots represent evolution of the canopy-layer temperature during period, covered by drone soundings, according to AWS observations.

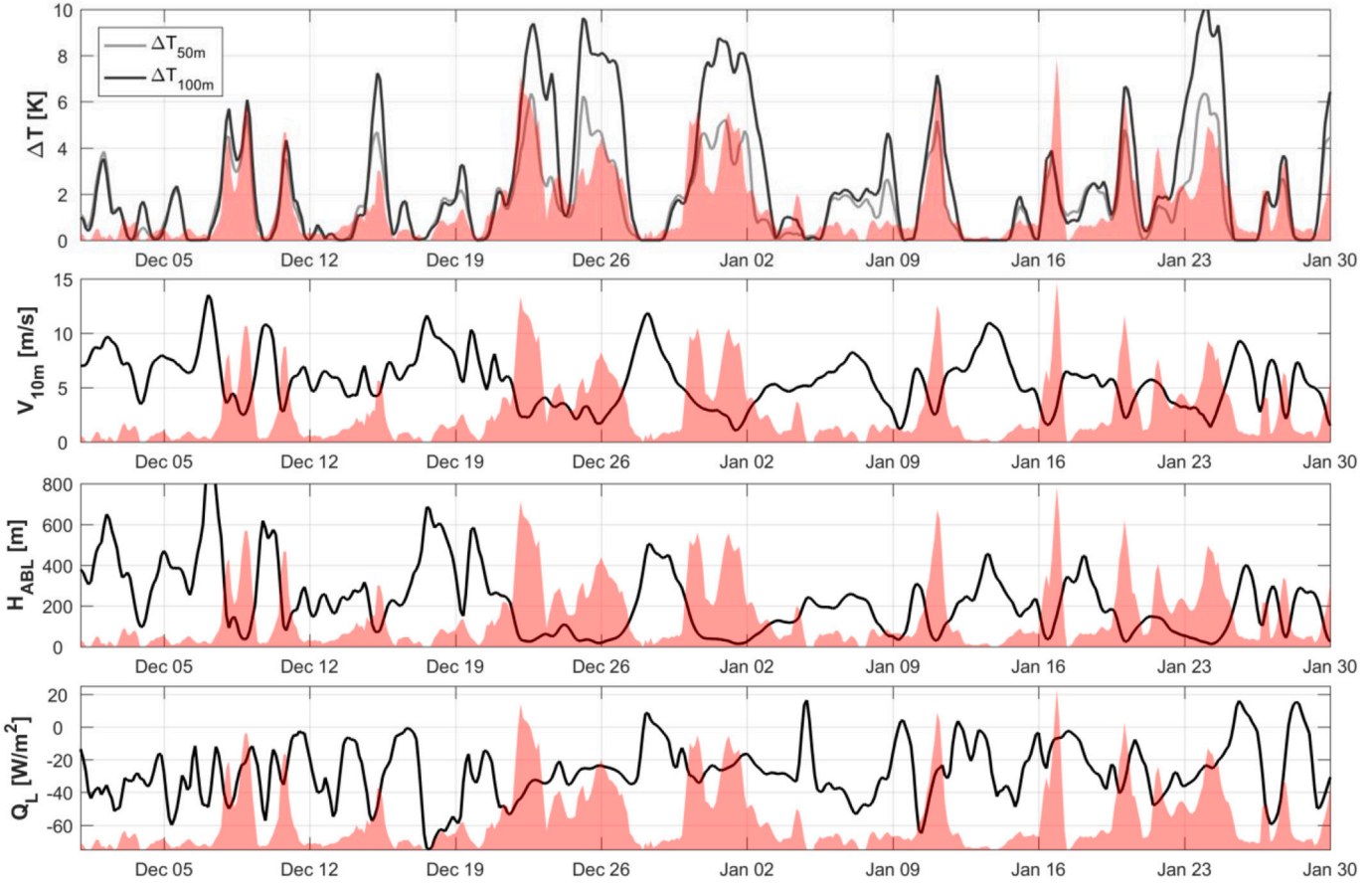

Fig. 10. Time series of the observed UCL UHI intensity based on the urban WMO AWS2 station readings (ΔT_{AWS2}) given by red shading in all subplots and selected ERA5 variables during December 2020–January 2021. (For interpretation of the references to color in this figure legend, the reader is referred to the web version of this article.)

ground-based inversion has emerged over the rural site. This inversion remained relatively weak, with θ difference not exceeding 1.5 K in the lowest 50 m (Fig. 7b,c). At the same time, a neutral layer with a height of 40–50 m existed in the city. UHI intensity was limited by 1.5 K, and the UHI vertical extent was 40–50 m. Such dynamics developed on the background of moderate wind speed (not exceeding 5 m/s in the lowest 50 m), which has been slowly decreasing during this observational period (Fig. 7d-e**)**. We did not find any systematic differences in the wind speed profiles over the selected sites. The profiles usually coincided at a height, and near the surface there were differences of different signs.

The IOP-3 data shows more details on ABL dynamics during a rapid cold spell accompanied by intense UCL UHI. Before the cold spell (January 9, 2021) the whole lower troposphere was well-mixed, and urban-rural temperature differences were negligible despite the wind speed was as low as only 2–3 m/s in the lowest 50 m (Fig. 8a, d). Rapid cooling the next day was accompanied by descending elevated inversion and strengthening of the ground-based inversion at the rural site R1 (Fig. 8b, c**)**. The temperature gradient at this site has exceeded 2 K in lower 50 m in the P3.12 case. The surface air temperature was 2 K lower at the WMO site. It indicates high localization of temperature anomalies in a thin surface layer. Perhaps, the R1 site has higher temperature because of some additional mixing created by passing cars, or due to local features of surface roughness and relief. Near-neutral stratification comprised the lowest 50–60 m of air at both urban sites, U1 and U2. Certain intra-urban variations (the U1 site was warmer than the U2 site) can be explained by differences in local settings of sites' footprints. Considering the northern winds (Fig. 8e,f**)**, the U2 site is more affected by winds from the industrial zone where large low- and mid-rise warehouse hangars are found. The U1 site is more exposed to winds from residential areas of the city, densely built up by mid- and high-rise apartment blocks. U1 site also experienced noticeably lower wind speed within the UBL (Fig. 8e,f**)**. The surface air temperature at the urban site does not drop until the end of the cold spell, but further cooling is observed for the rural site (Fig. 4b). Hence, UHI likely continued to intensify in the city against the strengthening rural ground-based inversion.

Data from IOPs-4 and IOP-5 illustrate ABL dynamics at the end of the cold spell (Fig. 4c,d). Due to nonstationary of conditions, here we consider urban/rural profiles for individual soundings instead of averaging between neighboring soundings (Fig. 9**)**. Initial temperature profile in IOP-4 was close to those observed during IOP-3, but with even stronger ground-based inversion and θ difference of >4 K in the lowest 50 m (Fig. 9a). In the city, as in previous cases, near-neutral stratification extended just from the surface at U2 site, resulting in UHI vertical extent about 40–50 m. The wind speed was lower than in previous cases, but still not zero (Fig. 9a). The further evolution of θ profiles clearly indicate that following warming was associated with warm air advection above the ABL. Nevertheless, it has also resulted in weakening of the rural ground-based inversion and warming of the rural WMO site exceeding that in the city. The UHI vertical extent was increasing. Evolution of the wind profiles identify the intensification of the ABL mixing during this short IOP. Almost similar dynamics was observed during IOP-5 (the cases P5.2 and P5.4 in Fig. 9). In that case, warming took place only in ABL and was likely associated with daytime solar heating (Fig. 3).

3.3. Boundary-layer control of intense UHIs

Surface heterogeneity has a significant impact on meteorology (wind, moisture, temperature), air quality, turbulent dynamics of the ABL. A concept of the blending height relates horizontal scales and intensity of surface heterogeneity (the UHI footprint) with the vertical extent of their boundary layer effects. The blending height determines a height at which influences of individual surface patches on vertical profiles or fluxes become indistinguishable (Wieringa, 1986; Claussen, 1991). The urban area could be considered as one of such patches, which may induce stronger anomalies than natural patches. Below the blending height UHI is distinct and make up urban climate (Barlow, 2014). The collected data directly reveal the UBL height in relation with the horizontal temperature difference (the UHI intensity) and vertical ABL stratification.

Our results clearly demonstrate a dominant role of the ground-based temperature inversions in formation and maintenance of pronounced UCL UHI. When such inversions develop in the rural boundary layer, near neutral or even unstable stratification persists in the UBL. Such ground-based temperature inversions accompanied by UCL and UBL UHI are usually observed during calm weather conditions which were preceded by radiative cooling. Yet, these two factors separately are necessary, but not sufficient for the UHI development. Performed observations revealed that calm wind speed even in cold weather may not be accompanied by UHI (see, e.g., P3.1-P3.3 profiles from IOP-3), and net long-wave radiation is not directly correlated with UHI intensity.

To confirm the climatological relevance of our results, we used UCL UHI observations in Nadym and ERA5 reanalysis for longer periods as descried in Section no. 2.4. Fig. 10 demonstrates that UCL UHI intensity is highly correlated with the strength of ground-based inversions, wind speed and the ABL height (Fig. 10). More details are given in (Table 2). The highest correlation coefficient is

Table 2
Correlation coefficients between canopy-layer UHI intensity and listed predictors. Color indicates absolute value of the correlation coefficient.

Urban site and period	ΔT_{50m}	ΔT_{100m}	ΔT_{200m}	ΔT_{300m}	V_{10m}	$\bar{V}_{50m}$	$\bar{V}_{100m}$	$\bar{V}_{200m}$	$\bar{V}_{300m}$	H_{ABL}	Q_L	V_{10m}^{obs}	F_W^{obs}
ΔT_{AWS1}, *P1*	0.56	0.60	0.58	0.57	-0.47	-0.47	-0.48	-0.48	-0.48	-0.48	-0.14	-0.52	0.61
ΔT_{AWS1}, *P2*	0.65	0.66	0.60	0.53	-0.58	-0.59	-0.60	-0.61	-0.61	-0.58	-0.12	-0.62	0.62
ΔT_{AWS2}, *P2*	0.70	0.70	0.61	0.53	-0.60	-0.61	-0.62	-0.63	-0.64	-0.59	-0.13	-0.65	0.63

found between the UHI intensity and the strength of temperature inversions, ΔT_z, in the lowest 50 or 100 m. The corresponding correlation coefficient reaches 0.7 for ΔT_{AWS2} in the P2 period., i.e., the strength of ground-based inversions explains 50% of UHI variability. Such correlation is smaller for AWS1 site, yet the ΔT_z remains the best reanalysis-based predictor for ΔT_{AWS1}. The correlations decrease if ΔT_z with z > 100 m is considered. Wind speed and the ABL height have significant, but less strong negative correlation with the UHI intensity as well. The correlation between UHI and the long-wave radiation balance is weak, yet many UHI events are foreshadowed by radiative cooling with strongly negative Q_L values (Fig. 10). The lag between peaks of radiative cooling and UHI is likely determined by the time needed for the rearrangement of the rural ABL into a strongly stable state with a ground-based inversion.

4. Discussion

Studies of UBL UHI are still scarce. Our study extends the UBL research towards a new geographical region of Siberian sub-Arctic and specific physical conditions of the high-latitude continental winter, characterized by almost absence of solar heating and presence of long-living stable boundary layers. Significant and distinct differences in the UBL vertical structure in the high- and mid/low-latitude cities could be disclosed through our study. Temperature inversions in the polar lower atmosphere impose strong constraints on the ABL height. UBL which developed in such stable conditions is mixed much better than rural ABL, but remains very thin, with a typical height of mixed layer about 50 m. Our instruments do not allow accurate quantification of rural ABL height, yet we expect that UBL is not considerably deeper than the rural ABL despite of being much better mixed. For temperate cities, deeper UBL and larger urban-rural differences in the ABL height were reported. For example, the ABL height was up to 45% (700 m) higher than that over the rural areas in Nashville, USA (Angevine et al., 2003). The mean difference was found to be 160 m; larger differences were observed in daytime. For Paris, France, Pal et al. (2012) reported the UBL height varied from 204 m (nighttime) to 1135 m (daytime). The most significant relative differences between urban and suburban sites (63 m or 45%) were observed at night. Several classic studies report a typical vertical extent of nocturnal UBL UHI in mid-latitude cities to be about 300 m, e.g. according to helicopter soundings in Montreal, Canada (Oke and East, 1971), New-York, USA (Bornstein, 1968) and Christchurch, New Zeeland (Tapper, 1990). In Moscow, Russia, the annual-mean nocturnal UHI vertical extent is about 100 m according to measurements at the Ostankino television tower (Lokoshchenko et al., 2016). Mesoscale meteorological models provide similar estimates (about 150 m) for the vertical extent of nocturnal UBL UHI for Moscow (Varentsov et al., 2018b) and Paris (Wouters et al., 2013).

At the first glance, the smaller vertical extent of UBL in Nadym in comparison to temperature cities can be explained by the smaller city size. However, the observed UCL UHI intensity in Nadym is comparable with that in much larger mid-latitude cities. Maximums of the UCL UHI intensity in Nadym may reach 7-8 K (for the AWS2 site). Thus, UHI in Nadym could be more intense than in cities from abovementioned UBL studies as well as other studied cities, such as the large Dutch cities (Steeneveld et al., 2011), Barcelona (Moreno-Garcia, 1994) and Bucharest (Cheval et al., 2009). Hence, due to the temperature inversions, UHI in a cold climate city in winter is characterized by the higher UCL UHI intensity and lower UBL vertical extent in comparison to typical mid-latitude city.

More constraint UBL in high latitudes may lead to severe air quality problems. UHI could be used as a convenient and practical indicator of atmospheric stability (temperature inversions) and therefore of low-level turbulence diffusion. Similar proxy associations have been recently suggested from satellite data analysis by (Li et al., 2018). Persistent wintertime temperature inversions strongly exacerbate air quality problems in high latitudes (Schmale et al., 2018). For example, one might consider winter air quality challenges in Fairbanks, Alaska (Tran and Mölders, 2011; Ye and Wang, 2020). Today, large international efforts are aimed to investigate and mitigate the problem of air pollution in the Arctic (ALPACA, https://alpaca.community.uaf.edu/; PACES, https://pacesproject.org/about). Our results highlight the importance of further in-depth investigation of the interaction between UHI and air quality in high latitudes.

Speaking about the limitations of our study, it is important to note that presented results do not provide full understanding of the physical drivers of the observed canopy-layer and ABL effects. Intense UHI in Nadym is observed in mid-winter, when urban-rural differences in evapotranspiration and solar radiation storage are negligible and cannot contribute to UHI appearance. Previous Arctic UHI studies suggested that anthropogenic heating is a primary driver of the wintertime UHI in high latitudes (Hinkel and Nelson, 2007; Konstantinov et al., 2018; Varentsov et al., 2018a). Same effect was also found with sensitivity model simulations for midlatitude winter conditions in Moscow, Russia (Varentsov et al., 2020). Yet, another possible mechanism could be driven by dynamical mixing, i.e. by the advection of stable air over a rougher area resulting in a positive thermal anomaly (Oke, 1982). Our observations in Nadym suggest that role of dynamical mixing may be underestimated in previous studies. Indeed, we observed that UCL and UBL UHI developed in stable conditions with weak but still non-zero wind speed (1.5–3 m/s in the lowest 50 m), including locations close to the upwind site of the city (U1 site in P1.1 case). Moreover, in IOP-3 we observed the intra-urban UBL evolution along the airflow adverting the city. Unfortunately, accurate quantification of the drivers associated with anthropogenic heating and dynamical mixing is not trivial, primary because detailed data on anthropogenic heat flux is not available for Nadym. More insides to this issue could be obtained in further studies using numerical modelling.

Finally, our study highlights the prospects of using new observation methods, in particular drones, for UBL monitoring and research. Drones are emerging tool for atmospheric sciences, yet they are still rarely used in urban areas, in particular because of strict limitations. The recently published United Nations U4SSC report (U4SSC, 2020) highlighted that with high mobility and low costs drones have found a wide range of applications in smart cities including environmental monitoring. Such new methods using drones can be recommended to be further include into the WMO's guide on urban observation (WMO, 2018) in its improved editions. Presented data was collected in extremely conditions using relatively cheap mass-market quadcopters. More advanced drone-based observation systems (e.g. Leuenberger et al., 2020; Segales et al., 2020) could be even more promising for monitoring applications

in urban areas and for providing necessary data for urban hydrometeorological, climate and environment services (WMO, 2019), in particular for air quality managed task.

5. Conclusion

Simultaneous observations of the urban heat island (UHI) in the urban canopy layer (UCL) and the vertical structure of the urban (UBL) and rural boundary layers were performed for a sub-Arctic city (Nadym, West Siberia, Russia) in very cold winter conditions. During five intensive observing periods that were distributed over 3 winters, we run simultaneous registration of urban and rural meteorological parameters. We applied novel observational techniques based on atmospheric sounding with unmanned drones, remote sensing with the meteorological temperature profiler MTP-5, and deployed a number of ground-based sensors and meteorological stations.

These new observations revealed details of UHI development in UCL and UBL, and allowed linking together the UCL UHI intensity, boundary layer stability and the UBL height. We found that pronounced UCL UHI with intensity up to 6-8 K appears when stable boundary layer with strong ground-based temperature inversion develops over rural areas. In such conditions, the UBL is less stratified than its rural counterpart (generally well-mixed), but is still very thin and limited in height by about 50 m. Correlation analysis based on longer UCL UHI observations and ERA5 reanalysis data further confirmed that the strength of the ground-based near-surface (50 m - 100 m above ground) temperature inversion is one of the strongest control factors for UHI in these conditions. Other widely acknowledged drivers, low wind speed and radiative cooling, are necessary, but not sufficient for UHI appearance.

Revealed linkage between UCL UHI and ground-based inversions highlights the relevance of UHI for air quality management in high-latitude cities. UCL UHI, which is simple to observe, could be used as proxy for ground-based inversions and associated air quality risks. Moreover, urban hydrometeorological, climate and environmental services could be further improved by introducing novel tools for ABL monitoring (drones, MTP) into the common practices of urban meteorological observations.

Funding

Experimental observations in Nadym were supported by Belmont Forum project SERUS (grant no. 1729) and Russian Foundation for Basic Research, project no. 20–55-71004. Development of the drone-based measuring complex and data processing routines performed by Mikhail Varentsov, Irina Repina and Arseniy Artamonov was supported by Russian Science Foundation, project no. 21–17-00249. Correlation analysis performed by Mikhail Varentsov was partially supported by the Russian Ministry of Education and Science as part of the program of the Moscow Center for Fundamental and Applied Mathematics under agreement no. 075–15–2019-1621, and by research and educational multidisciplinary school of Moscow State University “Brain, cognitive systems and artificial intelligence”.

CRediT authorship contribution statement

Mikhail Varentsov: Conceptualization, Data curation, Formal analysis, Investigation, Methodology, Resources, Software, Validation, Visualization, Writing – original draft, Writing – review & editing. **Pavel Konstantinov:** Conceptualization, Data curation, Investigation, Methodology, Resources, Writing – review & editing. **Irina Repina:** Conceptualization, Funding acquisition, Investigation, Methodology, Project administration, Resources, Supervision, Writing – review & editing. **Arseniy Artamonov:** Investigation, Data curation, Methodology, Resources, Writing – review & editing. **Alexander Pechkin:** Investigation, Resources, Writing – review & editing. **Andrei Soromotin:** Funding acquisition, Investigation, Project administration, Resources, Writing – review & editing. **Igor Esau:** Conceptualization, Funding acquisition, Methodology, Project administration, Supervision, Writing – original draft, Writing – review & editing. **Alexander Baklanov:** Conceptualization, Methodology, Supervision, Writing – review & editing.

Declaration of Competing Interest

The authors declare no conflict of interest.

Data availability

Data will be made available on request.

Acknowledgements

We are especially grateful for support of the administration and staff of Federal State Budgetary Institution “Ob-Irtysh Administration for Hydrometeorology and Environmental Monitoring”, and personally to Sergey Reshetov, engineer at WMO weather station in Nadym, for unvaluable help with experimental observations. We are also grateful to administration and staff of Scientific Center of Arctic Research (Salekhard, Russia) and its office in Nadym, and personally to Anton Sinitsky and Vasily Kobelev. We are thankful to Eugene Miller (ATTEX company) for his advices on interpreting the MTP-5 profiler data, and to Dr. Winston Chow (University of Singapore) for inspiring the idea of drone-based UBL research by his presentation at EGU-2016 conference.

References

Adkins, K., Wambolt, P., Sescu, A., Swinford, C., Macchiarella, N.D., 2020. Observational practices for urban microclimates using meteorologically instrumented unmanned aircraft systems. Atmosphere (Basel) 11. https://doi.org/10.3390/atmos11091008.

Angevine, W.M., White, A.B., Senff, C.J., Trainer, M., Banta, R.M., Ayoub, M.A., 2003. Urban-rural contrasts in mixing height and cloudiness over Nashville in 1999. J. Geophys. Res.-Atmos. 108, 1–10. https://doi.org/10.1029/2001jd001061.

Barlow, J.F., 2014. Progress in observing and modelling the urban boundary layer. Urban Clim. 10, 216–240. https://doi.org/10.1016/j.uclim.2014.03.011.

Barlow, J.F., Halios, C.H., Lane, S.E., Wood, C.R., 2015. Observations of urban boundary layer structure during a strong urban heat island event. Environ. Fluid Mech. 15, 373–398. https://doi.org/10.1007/s10652-014-9335-6.

Bell, T., Greene, B., Klein, P., Carney, M., Chilson, P., 2019. Confronting the boundary layer data gap: evaluating new and existing methodologies of probing the lower atmosphere. Atmos. Measure. Techn. Discuss. 1–23 https://doi.org/10.5194/amt-2019-453.

Benz, S.A., Bayer, P., Goettsche, F.M., Olesen, F.S., Blum, P., 2016. Linking surface urban Heat Islands with groundwater temperatures. Environ. Sci. Technol. 50, 70–78. https://doi.org/10.1021/acs.est.5b03672.

Bornstein, R.D., 1968. Observations of the urban Heat Island effect in new York City. J. Appl. Meteorol. 7, 575–582. https://doi.org/10.1175/1520-0450(1968)007<0575:OOTUHI>2.0.CO;2.

Brozovsky, J., Gaitani, N., Gustavsen, A., 2020. A systematic review of urban climate research in cold and polar climate regions. Renew. Sust. Energ. Rev. 110551 https://doi.org/10.1016/j.rser.2020.110551.

Chakraborty, T., Lee, X., 2019. A simplified urban-extent algorithm to characterize surface urban heat islands on a global scale and examine vegetation control on their spatiotemporal variability. Int. J. Appl. Earth Obs. Geoinf. 74, 269–280. https://doi.org/10.1016/j.jag.2018.09.015.

Cheval, S., Dumitrescu, A., Bell, A., 2009. The urban heat island of Bucharest during the extreme high temperatures of July 2007. Theor. Appl. Climatol. 97, 391–401. https://doi.org/10.1007/s00704-008-0088-3.

Chilson, P.B., Bell, T.M., Brewster, K.A., De Azevedo, G.B.H., Carr, F.H., Carson, K., et al., 2019. Moving towards a network of autonomous UAS atmospheric profiling stations for observations in the earth's lower atmosphere: the 3D mesonet concept. Sensors (Switzerland) 19. https://doi.org/10.3390/s19122720.

Claussen, M., 1991. Estimation of areally-averaged surface fluxes. Bound.-Layer Meteorol. 54, 387–410. https://doi.org/10.1007/BF00118868.

Davy, R., 2018. The climatology of the atmospheric boundary layer in contemporary global climate models. J. Clim. 31, 9151–9173. https://doi.org/10.1175/JCLI-D-17-0498.1.

Droste, A.M., Steeneveld, G.J., Holtslag, A.A.M., 2018. Introducing the urban wind island effect. Environ. Res. Lett. 13, 094007 https://doi.org/10.1088/1748-9326/aad8ef.

Esau, I., Miles, V., 2018. Exogenous drivers of surface urban Heat Islands in northern West Siberia. Geogr. Environ. Sustainabil. 11, 83–99. https://doi.org/10.24057/2071-9388-2018-11-3-83-99.

Esau, I., Miles, V.V., Davy, R., Miles, M.W., Kurchatova, A., 2016. Trends in normalized difference vegetation index (NDVI) associated with urban development in northern West Siberia. Atmos. Chem. Phys. 16, 9563–9577. https://doi.org/10.5194/acp-16-9563-2016.

Esau, I., Miles, V., Soromotin, A., Sizov, O., Varentsov, M., Konstantinov, P., 2021. Urban heat islands in the Arctic cities: an updated compilation of in situ and remote-sensing estimations. Adv. Sci. Res. 18, 51–57. https://doi.org/10.5194/asr-18-51-2021.

Ezau, I.N., Wolf, T., Miller, E.A., Repina, I.A., Troitskaya, Yu.I., Zilitinkevich, S.S., 2013. The analysis of results of remote sensing monitoring of the temperature profile in lower atmosphere in Bergen (Norway). Russ. Meteorol. Hydrol. 38, 715–722. https://doi.org/10.3103/S1068373913100099.

Fan, Y., Li, Y., Bejan, A., Wang, Y., Yang, X., 2017. Horizontal extent of the urban heat dome flow. Sci. Rep. 7, 1–10. https://doi.org/10.1038/s41598-017-09917-4.

Fan, Y., Li, Y., Yin, S., 2018. Non-uniform ground-level wind patterns in a heat dome over a uniformly heated non-circular city. Int. J. Heat Mass Transf. 124, 233–246. https://doi.org/10.1016/j.ijheatmasstransfer.2018.03.069.

Fan, Y., Wang, Q., Ge, J., Li, Y., 2020. Conditions for transition from a plume to a dome above a heated horizontal area. Int. J. Heat Mass Transf. 156, 1–12. https://doi.org/10.1016/j.ijheatmasstransfer.2020.119868.

Fedorov, R., Kuklina, V., Sizov, O., Soromotin, A., Prihodko, N., Pechkin, A., et al., 2021. Zooming in on Arctic urban nature: green and blue space in Nadym, Siberia. Environ. Res. Lett. 16 https://doi.org/10.1088/1748-9326/ac0fa3.

Gorlach, I.A., Kislov, A.V., Alekseeva, L.I., 2018. Experience of studying the vertical structure of an urban Heat Island based on satellite data. Izvestiya, Atmos. Oceanic Phys. 54, 1102–1109. https://doi.org/10.1134/s0001433818090189.

Han, J.Y., Baik, J.J., Lee, H., 2014. Urban impacts on precipitation. Asia-Pac. J. Atmos. Sci. 50, 17–30. https://doi.org/10.1007/s13143-014-0016-7.

Hersbach, H., Bell, B., Berrisford, P., Hirahara, S., Horányi, A., Muñoz-Sabater, J., et al., 2020. The ERA5 global reanalysis. Q. J. R. Meteorol. Soc. 146, 1999–2049. https://doi.org/10.1002/qj.3803.

Hinkel, K.M., Nelson, F.E., 2007. Anthropogenic heat island at Barrow, Alaska, during winter: 2001-2005. J. Geophys. Res.-Atmos. 112, 2001–2005. https://doi.org/10.1029/2006JD007837.

Hu, L., Brunsell, N.A., 2015. A new perspective to assess the urban heat island through remotely sensed atmospheric profiles. Remote Sens. Environ. 158, 393–406. https://doi.org/10.1016/j.rse.2014.10.022.

Järvi, L., Grimmond, C.S.B., McFadden, J.P., Christen, A., Strachan, I.B., Taka, M., et al., 2017. Warming effects on the urban hydrology in cold climate regions. Sci. Rep. 7, 1–8. https://doi.org/10.1038/s41598-017-05733-y.

Kadygrov, E.N., Pick, D.R., 1998. The potential for temperature retrieval from an angular-scanning single-channel microwave radiometer and some comparisons within situ observations. Meteorol. Appl. 5, 393–404. https://doi.org/10.1017/S1350482798001054.

Kadygrov, E.N., Miller, E.A., Nekrasov, V.V., Shaposhnikov, A.N., Troitsky, A.V., 2012. MTP5PE - New Instrument for Temperature Profiling in Polar Region. In: Proceedings of the 9th International Symposium on Tropospheric Profiling, L'Aquila, Italy., 1–3.

Kimball, S.K., Montalvo, C.J., Mulekar, M.S., 2020. Evaluating temperature measurements of the iMET-XQ, in the field, under varying atmospheric conditions. Atmosphere (Basel) 11. https://doi.org/10.3390/atmos11040335.

Klene, A.E., Nelson, F.E., Hinkel, K.M., 2013. Urban–rural contrasts in summer soil-surface temperature and active-layer thickness, Barrow, Alaska, USA. Polar Geogr. 36, 183–201. https://doi.org/10.1080/1088937X.2012.706756.

Konrad, T.G., Hill, M.L., Rowland, J.R., Meyer, J.H., 1970. A small, radio-controlled aircraft as A platform for meteorlogical sensors. APL Tech. Dig. 11–19.

Konstantinov, P., Varentsov, M., Esau, I., 2018. A high density urban temperature network deployed in several cities of Eurasian Arctic. Environ. Res. Lett. 13, 075007 https://doi.org/10.1088/1748-9326/aacb84.

Kral, S.T., Reuder, J., Vihma, T., Suomi, I., Haualand, K.F., Urbancic, G.H., et al., 2021. The innovative strategies for observations in the arctic atmospheric boundary layer project (ISOBAR) unique finescale observations under stable and very stable conditions. Bull. Am. Meteorol. Soc. 102, E218–E243. https://doi.org/10.1175/BAMS-D-19-0212.1.

Kumpula, T., Pajunen, A., Kaarlejärvi, E., Forbes, B.C., Stammler, F., 2011. Land use and land cover change in Arctic Russia: ecological and social implications of industrial development. Glob. Environ. Chang. 21, 550–562. https://doi.org/10.1016/j.gloenvcha.2010.12.010.

Lemonsu, A., Masson, V., 2002. Simulation of a summer urban breeze over Paris. Bound.-Layer Meteorol. 104, 463–490. https://doi.org/10.1023/A:1016509614936.

Leuenberger, D., Haefele, A., Omanovic, N., Fengler, M., Martucci, G., Calpini, B., et al., 2020. Improving high-impact numerical weather prediction with Lidar and drone observations. Bull. Am. Meteorol. Soc. 101, E1036–E1051. https://doi.org/10.1175/BAMS-D-19-0119.1.

Li, H., Meier, F., Lee, X., Chakraborty, T., Liu, J., Schaap, M., et al., 2018. Interaction between urban heat island and urban pollution island during summer in Berlin. Sci. Total Environ. 636, 818–828. https://doi.org/10.1016/j.scitotenv.2018.04.254.

Liu, J., Niyogi, D., 2019. Meta-analysis of urbanization impact on rainfall modification. Sci. Rep. 9, 1–14. https://doi.org/10.1038/s41598-019-42494-2.

Lokoshchenko, M.A., Korneva, I.A., 2015. Underground urban heat island below Moscow city. Urban Clim. 13, 1–13. https://doi.org/10.1016/j.uclim.2015.04.002.

Lokoshchenko, M.A., Korneva, I.A., Kochin, A.V., Dubovetsky, A.Z., Novitsky, M.A., Razin, P.Ye., 2016. Vertical extension of the urban heat island above Moscow. Dokl. Earth Sci. 466, 70–74. https://doi.org/10.1134/S1028334X16010128.

Mahrt, L., 2000. Surface heterogeneity and vertical structure of the boundary layer. Bound.-Layer Meteorol. 96, 33–62. https://doi.org/10.1023/A:1002482332477.
Miles, V., Esau, I., 2017. Seasonal and spatial characteristics of urban Heat Islands (UHIs) in northern west Siberian cities. Remote Sens. 9, 989. https://doi.org/10.3390/rs9100989.
Moreno-Garcia, M.C., 1994. Intensity and form of the urban heat island in Barcelona. Int. J. Climatol. 14, 705–710. https://doi.org/10.1002/joc.3370140609.
Neumann, P.P., Bartholmai, M., 2015. Real-time wind estimation on a micro unmanned aerial vehicle using its inertial measurement unit. Sens Actuat. A Phys. 235, 300–310. https://doi.org/10.1016/j.sna.2015.09.036.
Obu, J., Westermann, S., Bartsch, A., Berdnikov, N., Christiansen, H.H., Dashtseren, A., et al., 2019. Northern hemisphere permafrost map based on TTOP modelling for 2000–2016 at 1 km2 scale. Earth Sci. Rev. 193, 299–316. https://doi.org/10.1016/j.earscirev.2019.04.023.
Oke, T.R., 1982. The energetic basis of the urban heat island. Q. J. R. Meteorol. Soc. 108, 1–24. https://doi.org/10.1002/qj.49710845502.
Oke, T.R., 1995. The heat Island of the urban boundary layer: Characteristics, causes and effects. In: Wind Climate in Cities. Springer Netherlands, Dordrecht, pp. 81–107. https://doi.org/10.1007/978-94-017-3686-2_5.
Oke, T.R., 1998. An algorithmic scheme to estimate hourly heat island magnitude. In: Preprints, Second Symposium on Urban Environment, November 2–5, Albuquerque, NM, pp. 80–83.
Oke, T.R., East, C., 1971. The urban boundary layer in Montreal. Bound.-Layer Meteorol. 1, 411–437. https://doi.org/10.1007/BF00184781.
Oke, T.R., Mills, G., Christen, A., Voogt, J.A., 2017. Urban Climates. Cambridge University Press, Cambridge. https://doi.org/10.1017/9781139016476.
Pal, S., Xueref-Remy, I., Ammoura, L., Chazette, P., Gibert, F., Royer, P., et al., 2012. Spatio-temporal variability of the atmospheric boundary layer depth over the Paris agglomeration: an assessment of the impact of the urban heat island intensity. Atmos. Environ. 63, 261–275. https://doi.org/10.1016/j.atmosenv.2012.09.046.
Palomaki, R.T., Rose, N.T., van den Bossche, M., Sherman, T.J., De Wekker, S.F.J., 2017. Wind estimation in the lower atmosphere using multirotor aircraft. J. Atmos. Ocean. Technol. 34, 1183–1191. https://doi.org/10.1175/JTECH-D-16-0177.1.
Qian, Y., Chakraborty, T.C., Li, J., Li, D., He, C., Sarangi, C., et al., 2022. Urbanization impact on regional climate and extreme weather: current understanding, uncertainties, and future research directions. Adv. Atmos. Sci. https://doi.org/10.1007/s00376-021-1371-9.
Schmale, J., Arnold, S.R., Law, K.S., Thorp, T., Anenberg, S., Simpson, W.R., et al., 2018. Local Arctic air pollution: A neglected but serious problem. Earths Future 6, 1385–1412. https://doi.org/10.1029/2018EF000952.
Segales, A.R., Greene, B.R., Bell, T.M., Doyle, W., Martin, J.J., Pillar-Little, E.A., et al., 2020. The CopterSonde: an insight into the development of a smart unmanned aircraft system for atmospheric boundary layer research. Atmos. Meas. Tech. 13, 2833–2848. https://doi.org/10.5194/amt-13-2833-2020.
Sekula, P., Zimnoch, M., Bartyzel, J., Bokwa, A., Kud, M., Necki, J., 2021. Ultra-light airborne measurement system for investigation of urban boundary layer dynamics. Sensors 21. https://doi.org/10.3390/s21092920.
Sizov, O., Ezhova, E., Tsymbarovich, P., Soromotin, A., Prihod'Ko, N., Petäjä, T., et al., 2021. Fire and vegetation dynamics in Northwest Siberia during the last 60 years based on high-resolution remote sensing. Biogeosciences 18, 207–228. https://doi.org/10.5194/bg-18-207-2021.
Sizov, O.S., Lobotrosova, S.A., 2016. Features of revegetation of drift sand sites in the northern taiga subzone of Western Siberia. Earth's Cryosp. 20, 3–13. https://doi.org/10.21782/KZ1560-7496-2016-3(3-13).
Soromotin, A.V., Ezau, I.N., Sizov, O.S., Lobostrova, S.A., Frank, K.A., 2021. Microclimatic features of sand dunes in northern taiga in Western Siberia. Meteorol. Gidrol. 88–100. https://doi.org/10.52002/0130-2906-2021-8-88-100.
Stammler, F., Sidorova, L., 2015. Dachas on permafrost: the creation of nature among Arctic Russian city-dwellers. Polar Record 51, 576–589. https://doi.org/10.1017/S0032247414000710.
Steeneveld, G.J., Koopmans, S., Heusinkveld, B.G., Van Hove, L.W.A., Holtslag, A.A.M., 2011. Quantifying urban heat island effects and human comfort for cities of variable size and urban morphology in the Netherlands. J. Geophys. Res.-Atmos. 116, 1–14. https://doi.org/10.1029/2011JD015988.
Tapper, N.J., 1990. Urban influences on boundary layer temperature and humidity: results from Christchurch, New Zealand. Atmos. Environ. Part B. Urban Atmos. 24, 19–27. https://doi.org/10.1016/0957-1272(90)90005-F.
Tikhomirov, A.B., Lesins, G., Drummond, J.R., 2021. Drone measurements of surface-based winter temperature inversions in the high Arctic at Eureka. Atmos. Meas. Tech. 14, 7123–7145. https://doi.org/10.5194/amt-14-7123-2021.
Tran, H.N.Q., Mölders, N., 2011. Investigations on meteorological conditions for elevated PM2.5 in Fairbanks, Alaska. Atmos. Res. 99, 39–49. https://doi.org/10.1016/j.atmosres.2010.08.028.
U4SSC, 2020. Accelerating City Transformation Using Frontier Technologies: A U4SSC Deliverable. Geneva. Available at: https://www.itu.int/go/u4SSC.
Varentsov, M., Konstantinov, P., Baklanov, A., Esau, I., Miles, V., Davy, R., 2018a. Anthropogenic and natural drivers of a strong winter urban heat island in a typical Arctic city. Atmos. Chem. Phys. 18, 17573–17587. https://doi.org/10.5194/acp-18-17573-2018.
Varentsov, M., Wouters, H., Platonov, V., Konstantinov, P., 2018b. Megacity-induced Mesoclimatic effects in the lower atmosphere: A modeling study for multiple summers over Moscow, Russia. Atmosphere (Basel) 9, 50. https://doi.org/10.3390/atmos9020050.
Varentsov, M., Samsonov, T., Demuzere, M., 2020. Impact of urban canopy parameters on a Megacity's modelled thermal environment. Atmosphere (Basel) 11, 1349. https://doi.org/10.3390/atmos11121349.
Varentsov, M., Stepanenko, V., Repina, I., Artamonov, A., Bogomolov, V., Kuksova, N., et al., 2021a. Balloons and quadcopters: Intercomparison of two low-cost wind profiling methods. Atmosphere (Basel) 12, 380. https://doi.org/10.3390/atmos12030380.
Varentsov, M., Stepanenko, V., Repina, I., Artamonov, A., Bogomolov, V., Kuksova, N., et al., 2021b. Balloons and quadcopters: Intercomparison of two low-cost wind profiling methods. Atmosphere (Basel) 12, 380. https://doi.org/10.3390/atmos12030380.
Varentsov, M.I., Yu Artamonov, A., Pashkin, A.D., Repina, I.A., 2019. Experience in the quadcopter-based meteorological observations in the atmospheric boundary layer. IOP Conf. Ser. Earth Environ. Sci. 231, 012053 https://doi.org/10.1088/1755-1315/231/1/012053.
Vasiliev, A.A., Drozdov, D.S., Gravis, A.G., Malkova, G.V., Nyland, K.E., Streletskiy, D.A., 2020. Permafrost degradation in the Western Russian Arctic. Environ. Res. Lett. 15, 45001. https://doi.org/10.1088/1748-9326/ab6f12.
Vogelezang, D.H.P., Holtslag, A.A.M., 1996. Evaluation and Model Impacts of Alternative Boundary-Layer Height Formulations, pp. 245–269. Available at: https://doi.org/10.1007/BF02430331.
Voogt, J.A., Oke, T.R., 2003. Thermal remote sensing of urban climates. Remote Sens. Environ. 86, 370–384. https://doi.org/10.1016/S0034-4257(03)00079-8.
Wetzel, C., Brümmer, B., 2011. An Arctic inversion climatology based on the European Centre reanalysis ERA-40. Meteorol. Z. 20, 589–600. https://doi.org/10.1127/0941-2948/2011/0295.
Wieringa, J., 1986. Roughness-dependent geographical interpolation of surface wind speed averages. Q. J. R. Meteorol. Soc. 112, 867–889. https://doi.org/10.1002/qj.49711247316.
WMO, 2018. Chapter 9. Urban observations. In: Guide to Meteorological Instruments and Methods of Observation Volume III - Observing Systems. World Meteorological Organization, Geneva, pp. 371–399.
WMO, 2019. Guidance on Integrated Urban Hydro-Meteorological, Climate and Environmental Services. World Meteorological Organization, Geneva. Available at: https://library.wmo.int/doc_num.php?explnum_id=9903.
Wood, C.R., Järvi, L., Kouznetsov, R.D., Nordbo, A., Joffre, S., Drebs, A., et al., 2013. An overview of the urban boundary layer atmosphere network in Helsinki. Bull. Am. Meteorol. Soc. 94, 1675–1690. https://doi.org/10.1175/BAMS-D-12-00146.1.
Wouters, H., de Ridder, K., Demuzere, M., Lauwaet, D., van Lipzig, N.P.M., 2013. The diurnal evolution of the urban heat island of Paris: A model-based case study during summer 2006. Atmos. Chem. Phys. 13, 8525–8541. https://doi.org/10.5194/acp-13-8525-2013.
Xiao, X.D., Dong, L., Yan, H., Yang, N., Xiong, Y., 2018. The influence of the spatial characteristics of urban green space on the urban heat island effect in Suzhou Industrial Park. Sustain. Cities Soc. 40, 428–439. https://doi.org/10.1016/j.scs.2018.04.002.

Ye, L., Wang, Y., 2020. Long-term air quality study in Fairbanks, Alaska: air pollutant temporal variations, correlations, and pm2.5 source apportionment. Atmosphere (Basel) 11, 2010–2011. https://doi.org/10.3390/atmos11111203.

Yu, Q., Epstein, H.E., Engstrom, R., Shiklomanov, N., Strelestskiy, D., 2015. Land cover and land use changes in the oil and gas regions of northwestern Siberia under changing climatic conditions. Environ. Res. Lett. 10 https://doi.org/10.1088/1748-9326/10/12/124020.

Zhou, D., Xiao, J., Bonafoni, S., Berger, C., Deilami, K., Zhou, Y., et al., 2018. Satellite remote sensing of surface urban Heat Islands: progress, challenges, and perspectives. Remote Sens. 11, 48. https://doi.org/10.3390/rs11010048.